

pubs.acs.org/cm Article

Pentiptycene-Containing Polybenzoxazole Membranes with a Crosslinked Unimodal Network Structure for High-Temperature Hydrogen Separations

Si Li, Ziwei Dai, Tao Wang, Zihan Huang, and Ruilan Guo*



Cite This: Chem. Mater. 2022, 34, 9577-9588



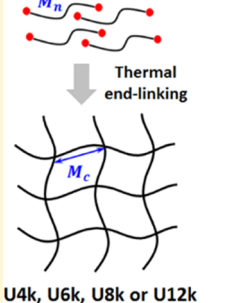
ACCESS I

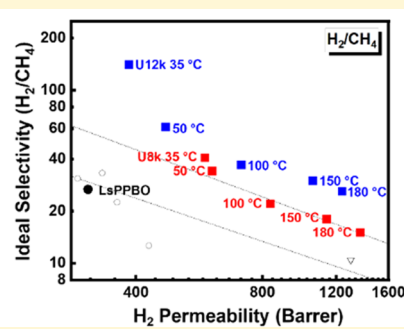
III Metrics & More

Article Recommendations

Supporting Information

ABSTRACT: Membranes with excellent stability and stable separation performance under complex or harsh conditions are essential to a successful membrane separation system. Herein, we report a new design of robust crosslinked polymer membranes with unimodal network structures that exhibit superior separation performance surpassing the 2008 upper bound for $\rm H_2/CH_4$ separation at both ambient (35 °C) and elevated temperatures (up to 180 °C). The crosslinked membranes are based on pentiptycene-containing polybenzoxazole (PPBO) structures prepared via a new controlled crosslinking method, i.e., end-linking of telechelic PPBO oligomers with controlled molecular weight and a thermally curable phenylethynyl group at the chain ends. Using the





synthesized oligomer with various molecular weights (4000–12 000 g/mol), the consequent crosslink density of unimodal networks was comprehensively varied. A nonlinear relationship between membrane properties and the crosslink density is observed, which is ascribed to the competing effects between crosslinking-induced densification and the formation of bulky benzoxazole and phenyl groups at the crosslink joints. The concept of unimodal networks exemplifies a novel approach that is able to finely tailor crosslinked microstructures and consequently maximize the membrane separation performance at elevated temperatures.

1. INTRODUCTION

The past decades witnessed intensified research interest in membrane-mediated gas separation and its rapid transformation into a commercial reality. Since the late 1970s, the gas separation membrane market entered its booming era and is projected to reach \$2.61 billion by 2022 with an average annual increase rate of 7-8%. The appealing features of membrane separation technology, i.e., simple operation, low energy and capital costs, and small footprint, found a prospective future in various processes, such as hydrogen recovery, natural gas purification, and air separation.^{2,3} For polymer gas separation membranes, while the challenge of permeability-selectivity trade-off seems to be tackled by the large number of new polymers developed through decades of research that have pushed the limits further toward the upper right side in Robeson's upper bound plots, 4-7 only around 10 kinds of polymer materials (e.g., polysulfone, polyimide, and polyphenylene oxide) have made it to commercial applications although hundreds of highly permeable and selective polymers have been developed and evaluated for gas separation membranes.8 The major hurdle to the practical implementation of new polymer membrane materials is their stability/ durability under harsh conditions, such as plasticization and physical aging, where membranes lose their size-sieving capability upon exposure to condensable gases or high

temperatures or suffer from greatly reduced permeability upon aging. 8,9

Crosslinking represents one of the most competent approaches to improve membrane durability under harsh conditions (e.g., high temperatures) and provides resistance to plasticization and physical aging by forming an interlocked network with restrained segmental motion. 10-13 However, the much-improved membrane stability is always accompanied by significantly reduced gas permeability with little gain in selectivity due to crosslinking-induced membrane densification, which greatly reduces the gas transport pathways required for high permeability. It is also frequently observed that crosslinked membranes show unpredictable transport properties. This discrepancy is mainly due to the uncontrolled, random crosslinking processes used to prepare crosslinked membranes, where crosslinking reactions occur randomly within polymer chains resulting in very complicated crosslinked network structures. Moreover, the structure

Received: July 15, 2022 Revised: October 13, 2022 Published: October 26, 2022





tunability of randomly crosslinked membranes is extremely limited with only one adjustable parameter, the crosslink density, which, however, often failed to predict and explain the gas transport properties of crosslinked membranes. For example, Berean et al. attributed the optimized separation performance to the crosslink density. Is fahani et al. reported decreased gas permeability with increasing crosslink density, and a similar trend was observed in other reports. However, a study by Lin et al. objected to the conclusion that the crosslink density dominates the permeability and diffusion coefficient. From a fundamental point of view, the intricate network structure from the random crosslinking process put off the chance to reveal the gas-transport mechanism in crosslinked membranes.

To fill this fundamental knowledge gap, we developed a controlled end-linking approach, 22,23 where telechelic oligomers with a precisely controlled molecular weight (MW) are end-linked via thermal curing reactions between the terminal functional groups (such as epoxy) to produce model polymer network structures with a specifically defined crosslink density and crosslink inhomogeneity, such as unimodal networks (e.g., uniform chain length between crosslinks determined by the oligomer molecular weight). We demonstrated that crosslinked unimodal polyimide membranes developed from the thermal end-linking of phenylethynyl-terminated Matrimid-like oligomers exhibited remarkably improved gas permeability along with wellpreserved selectivity compared with the uncrosslinked linear control, resulting in a nearly horizontal improvement against the upper bound along with excellent membrane stability.²⁴ In this study, we extend the model network concept to a highperformance polymer series, i.e., pentiptycene-containing polybenzoxazoles (PPBOs),²⁵ to examine the applicability of the model network concept as well as to produce highly permeable and selective crosslinked gas separation membranes. Figure 1 summarizes the preparation of crosslinked PPBO

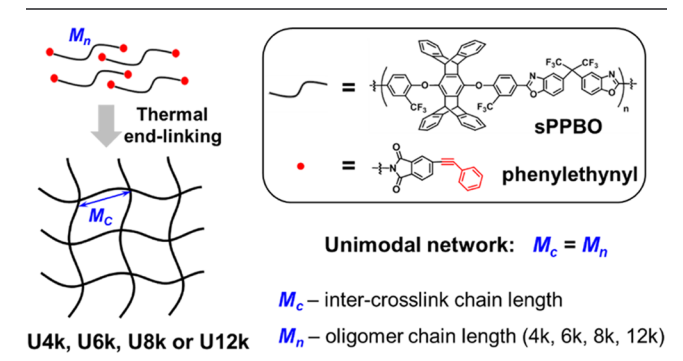


Figure 1. End-linking of phenylethynyl-terminated sPPBO oligomers to form crosslinked membranes with a unimodal network structure, wherein the crosslink density, described by the inter-crosslink chain length $(M_c$, g/mol), is determined and controlled by the chain length (M_n) of the telechelic sPPBO oligomers.

membranes with a unimodal network structure. A series of telechelic pentiptycene-containing polybenzoxazole oligomers (sPPBO) with controlled MW ranging from 4000 to 12 000 g/mol are synthesized and terminated at both ends with thermally curable phenylethynyl groups. Different from the conventional random crosslinking process, crosslinking reactions occur exclusively at the chain ends of sPPBO oligomers, i.e., thermal end-linking of phenylethynyl groups. Conse-

quently, crosslinked membranes with a well-defined unimodal network structure are obtained, wherein the crosslink density can be unambiguously described by the inter-crosslink chain length ($M_{\rm c}$) equaling the oligomer chain length ($M_{\rm n}$). In this study, sPPBO unimodal network membranes with varied crosslink densities are prepared and examined in terms of microstructure, physical properties, and gas permeation. Correlations between the crosslinked structure and transport properties are elucidated, which signifies new strategies to manipulate the microstructure of crosslinked films and maximize their separation performance, particularly at high temperatures.

2. EXPERIMENT

2.1. Materials. 2,2′-Bis(3-amino-4-hydroxyphenyl) hexafluoropropane (6FAP, >98.5%, Akron Polymer Systems) was oven dried for 12 h at 65 °C in vacuum before use. 4-Phenylethynylphthalic anhydride (PEPA, >99%, Akron Polymer Systems), anhydrous 1-methyl-2-pyrrolidinone (NMP, 99.5%, Sigma-Aldrich), anhydrous N,N-dimethylformamide (DMF, 99.8%, Sigma-Aldrich), dichloromethane (DCM, 99.5%, Sigma-Aldrich), acetonitrile (≥99.5%, Sigma-Aldrich), thionyl chloride (≥99%, Sigma-Aldrich), potassium carbonate (≥99%, Sigma-Aldrich), benzyl bromide (98%, Sigma-Aldrich), palladium on activated charcoal (10% Pd basis, Sigma-Aldrich) chlorotrimethylsilane (TMCS, ≥99%, Sigma-Aldrich), 1,2-dichlorobenzene (o-DCB, 99.0%, Sigma-Aldrich), 4-fluoro-3-(trifluoromethyl) benzoic acid (98.0%, Matrix Scientific), and anhydrous pyridine (≥99.8%, EMD Chemicals Inc.) were used directly.

2.2. Synthesis of Pentiptycene-Containing Diacid Chloride (PPDC). Pentiptycene-based diacid chloride, PPDC (4), was prepared by the chloroformylation of pentiptycene dicarboxylic acid (3) reduced from the dibenzo compound (2) following Scheme 1. Pentiptycene diol (PPOH) was synthesized following the procedures reported in our previous publication.²⁷ Meta-substituted trifluoromethyl neighboring the pentiptycene units was introduced via aromatic nucleophilic substitution between the pentiptycene diol and the fluoro compound (1) to improve the solubility and reactivity of the pentiptycene-containing monomer. The detailed synthesis procedures are as follows:

2.2.1. Synthesis of CF_3 -Containing Fluoro-Compound (1). 4-Fluoro-3-(trifluoromethyl) benzoic acid (5.0 g, 24 mmol), 1-(bromomethyl)benzene (4.11 g, 24 mmol), predried K_2CO_3 (6.64 g, 48 mmol), and 72 mL of acetonitrile (MeCN) were charged into a flame-dried, two-neck flask (250 mL) equipped with a stir bar. The reaction mixture was stirred under N_2 for 11 h at 80 °C before pouring into 80 mL of deionized (DI) water after cooling to ambient temperature. The aqueous solution was extracted three times using 200 mL of DCM. The organic phase was collected and dried using anhydrous Na_2SO_4 , followed by rotating evaporation at 45 °C to remove the DCM solvent. After vacuum drying for 12 h at 60 °C, fluoro-compound (1) was obtained as a viscous yellowish liquid.

2.2.2. Synthesis of Pentiptycene-Containing Dibenzo Compound (2). A two-neck flask equipped with a stir bar and condenser was charged with pentiptycene diol (PP-OH) (6.95 g, 15 mmol), fluoro-compound (1) (10.75 g, 35 mmol), predried K₂CO₃ (6.23 g, 45 mmol), and anhydrous DMF (70 mL) in order. Under an N₂ purge, the mixture was stirred for 10 h at 120 °C. After naturally cooling down, the suspension

Scheme 1. Synthesis of the Pentiptycene-Containing Diacid Chloride (PPDC) Monomer (4)

Scheme 2. Synthesis of Phenylethynyl-Terminated Polybenzoxazole Oligomers (sPPBO) with a Controlled Molecular Weight

was transferred to a methanol/water mixture (600 mL, 1:1, v/v), stirred vigorously for 1 h, and then filtered and dried for 12 h at 100 °C under vacuum. The obtained white solids were recrystallized twice in anhydrous DMF at 145 °C, forming clean snow-white solid products with good yields (>80%).

2.2.3. Synthesis of Pentiptycene-Containing Dicarboxylic Acid (3). The pentiptycene-containing dibenzo compound (2) (5 g, 4.9 mmol), DI water (100 mL), DMSO (100 mL), and potassium hydroxide (20 g) were charged into a two-neck flask

equipped with a stir bar in sequence. The mixture was refluxed for 3 days at 130 $^{\circ}\text{C}$ under N_2 protection, and the top transparent organic layer was collected. Hydrochloric acid (36 mL; 12 mol/L) was diluted with 120 mL of DI water and added dropwise into the collected hot solution. The protonated dispersion was stirred in high speed at 100 $^{\circ}\text{C}$ for 1 day, followed by filtration and drying overnight at 120 $^{\circ}\text{C}$ to afford the final products as fine snow-white powdered products.

2.2.4. Synthesis of Pentiptycene-Containing Diacid Chloride (4). Pentiptycene-containing dicarboxylic acid (3) (5 g, 6.0 mmol) and 18 mL of thionyl chloride were added into a flame-dried single-neck flask with a condenser. The reaction mixture was refluxed at 90 °C for 16 h. Upon cooling, the solution was rotavap-dried at 40 °C under reduced pressure followed by vacuum drying for 12 h at 60 °C to afford the final product as a white powder.

2.3. Synthesis of Phenylethynyl End-Capped Pentiptycene-Based Polybenzoxazole Oligomers (sPPBO) with Systematically Varied Molecular Weights. Scheme 2 shows the synthesis of phenylethynyl-terminated sPPBO oligomers with a systematically tuned MW. First, a series of amine-ended pentiptycene-containing poly(hydroxyl amide) oligomers (PPHA-NH₂) of a defined MW varying from 4000 to 12 000 g/mol was prepared by polycondensation between PPDC and 6FAP in predetermined ratios by the in situ silylation method following our previous report.²⁸ The final phenylethynyl-terminated sPPBO oligomers were obtained via end-capping PPHA-NH2 oligomers with crosslinkable phenylethynyl groups via condensation between amine end groups and the end-capping reagent, PEPA, followed by thermal cyclodehydration of the solution. The molecular weight of PPHA-NH₂ oligomers was controlled by offsetting the stoichiometric ratio of PPDC/6FAP, where 6FAP was in excess, to control the molecular weight and provide amine terminal groups for endcapping with PEPA. The feed ratio of PPDC/6FAP was calculated from the Carothers equation based on the target molecular weight of PPHA-NH₂ oligomers, as listed in Table S1.

An example of the synthesis of the sPPBO oligomer (8k) is as follows: to a dry, 100 mL three-neck round-bottom flask with a mechanical stirrer under N2, 6FAP (1.0000 g, 2.73 mmol) and 10 mL of anhydrous NMP were added and stirred until they dissolved; then, 1.4 mL of TMCS (11.2 mmol) and 0.9 mL of pyridine (11.7 mmol) were added and stirred for 2 h at room temperature to complete the silylation of 6FAP before PPDC (2.0631 g, 2.35 mmol), and 10 mL of anhydrous NMP and 0.3 mL of anhydrous pyridine were added. The reaction solution was stirred at room temperature for 16 h to form a solution of silylated PPHA-NH2 oligomers, which was precipitated and stirred overnight in a methanol/water mixture (1:1, volume ratio). The obtained PPHA-NH₂ oligomers were vacuum filtered, collected, and dried at 120 °C in a vacuum oven overnight. For endcapping and cyclodehydration, dry PPHA-NH₂ oligomers (~2.8 g) were dissolved in 16 mL of anhydrous NMP and silylated with 1.4 mL of TMCS and 1.2 mL of pyridine. After the completion of silylation in 2 h, PEPA (0.1858 g, 0.75 mmol) was introduced with another 24 h of stirring to form phenylethynyl-terminated PPHA oligomers. Finally, solution thermal cyclodehydration was performed in situ at 195 °C for 20 h using 4 mL of o-DCB to azeotropically convert PPHA oligomers into sPPBO oligomers. The sPPBO oligomers were precipitated and stirred overnight in a methanol/water mixture (1:1, v/v), filtered, repeatedly washed using DI water, and dried for 12 h at 160 °C in vacuum. Chemical structures and the number-average molecular weight (M_p) of the synthesized sPPBO oligomers were determined using proton nuclear magnetic resonance spectroscopy (1H NMR) and end-group analysis. The M_n values of sPPBO oligomers were determined to be 4100, 5800, 8500, and 11 700 g/mol, denoted as 4k, 6k, 8k, and 12k, respectively. A highmolecular-weight, linear pentiptycene-containing polybenzoxazole without end-capped functional groups, denoted as LsPPBO, was synthesized as a linear control using protocols similar to that mentioned above with an exactly 1:1 PPDC/6FAP feed ratio. The chemical structure of LsPPBO was confirmed using ¹H NMR (400 MHz, CDCl₃).

2.4. Thermal End-Linking and Membrane Fabrication. All of the crosslinked films were prepared in a Thermolyne F47925-80 Muffle Furnace (Thermo Scientific) using predetermined thermal protocols under nitrogen protection. In a typical case, 7.5 wt % oligomer solution (0.3 g of oligomers dissolved in 4 g of NMP at 100 °C) was filtered hot through a 0.45 μ m PTFE syringe filter before solution casting. The clear solution was cast onto a leveled aluminumfoil-covered glass plate in the furnace at 100 °C. The crosslinked films were obtained by thermal treatment as follows: 10 °C/min from 100 to 180 °C, then 4 °C/min to 300 °C (Ramp I) to slowly remove the solvent, followed by a 2 h isotherm at 300 °C (Isotherm I), then increased to 400 °C (crosslink temperature) at 50 °C/min (Ramp II), followed by 1 h at 400 °C (Isotherm II) to obtain fully crosslinked sPPBO films. The thermally crosslinked membrane was peeled off the aluminum foil after the hot furnace was naturally cooled down (cooling rate <10 °C/min) to ambient temperature. The membrane thickness was determined by a digital micrometer in the range between 40 and 60 μ m. The prepared crosslinked membranes are referred to as U4k, U6k, U8k, and U12k, respectively, wherein U signifies the unimodal network structure with even inter-crosslink chain length (M_c) values, followed by the value of M_n of sPPBO oligomers used for membrane preparation (i.e., $M_c = M_n$).

The completion degree of thermal crosslinking was determined by detecting the weight loss of the crosslinked films in hot NMP via gel fraction experiments. Specifically, 0.05-0.1 g of crosslinked film was dried and weighed before (W_i) , and after (W_d) being soaked in 50-100 mL of NMP at 150 °C for a week. The gel fraction of the cured films was determined as follows:

gel fraction =
$$\frac{W_{\rm d}}{W_{\rm i}} \times 100\%$$

As a linear control to provide reliable comparisons, a high-MW LsPPBO polymer was cast into thin films via the solution-casting method, while the 7.5 wt % polymer solution was prepared by the same method. The solution was spread on a leveled glass plate, dried under a 120 V infrared lamp (Staco Energy Products Co.) overnight, and then immersed for 24 h in methanol. The film was dried at 160 °C for 12 h in a vacuum oven to form linear sPPBO membranes, denoted as LsPPBO.

2.5. Characterization. ¹H NMR spectroscopy was performed on a Bruker AVANCE III HD 400 spectrometer using deuterated chloroform or dimethylsulfone (DMSO-*d*₆) as the solvent. Thermogravimetric analysis (TGA) was performed on a TGA Q500 (TA Instruments) under nitrogen (50 mL/min). The crosslinked films were tested at a heating rate of 10 °C/min up to 800 °C. The responses of telechelic oligomers during thermal treatment was tracked by applying the same thermal protocols as those in the preparation of crosslinked membranes, as discussed in Section 2.4.

Differential scanning calorimetry (DSC) analyses were performed on a DSC Q2000 (TA Instruments). Under a 50 mL/min nitrogen purge, the test was performed at a heating/

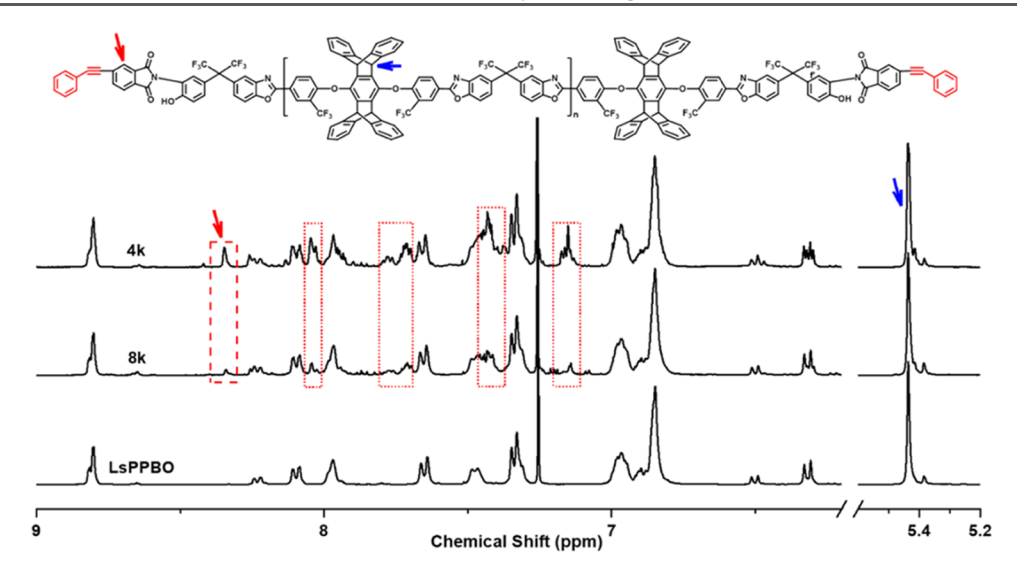


Figure 2. ¹H NMR spectra of representative sPPBO oligomers (4k and 8k) and LsPPBO (CDCl₃, 400 MHz). End group peaks are highlighted in dashed/dotted frames (peak assignments are shown in Figure S1). Molecular weight of the oligomers is determined from the integration ratio between select end-group peak (red arrow) and the main chain peak (blue arrow).

cooling rate of 10 °C/min ramping from ambient temperature to 300 °C in the first cycle and from 100 to 450 °C for the second cycle. Data from the second heating cycle were used to analyze the glass transition temperature $(T_{\rm g})$ of the oligomers and track the exothermic thermal curing reaction of phenylethynyl end groups.

Fourier-transform infrared (FTIR) spectra were obtained using a JASCO FT-IR 6300 spectrometer. Under attenuated total reflection (ATR) mode, all of the oligomers, crosslinked films, and linear controls were analyzed using 64 scans under a resolution of 4 cm⁻¹.

Wide-angle X-ray scattering (WAXS) was recorded on a Bruker D8 Advance Davinci diffractometer using Cu $K\alpha$ radiation (40 mA and 40 kV with a wavelength (λ) of 1.54 Å) with a step size of 0.02°/step and a scan speed of 7 s/step in the 5–45° (2 θ) range. The average d-spacing (d) was calculated from Bragg's law:

$$d = \frac{n\lambda}{2\sin\theta}$$

Crosslinked membrane densities were measured in DI water at ambient temperature with an analytical balance (ML204, Mettler Toledo) combined with a density kit using dry films by the buoyancy method. Then, the fraction-free volume (FFV) was calculated from the experimentally determined density:^{27,28}

$$FFV = \frac{V - V_0}{V}$$

where the specific volume (V) of the polymer is calculated from the experimentally determined density and the occupied volume (V_0) is estimated by the Bondi's group contribution method as follows:

$$V_0 = 1.3 \sum V_{\text{vdW}}$$

where $V_{\rm vdW}$ is the van der Waals volume of a single repeating unit and fraction of the end groups according to their calculated molecular weights.

Pure gas permeabilities (P, in Barrer) of H₂, CH₄, N₂, O₂, and CO₂ at 35 °C were obtained via the constant-volume,

variable-pressure method.⁸ The fully dried film was loaded and degassed in the gas cell on both sides for at least 12 h. Before permeation tests, the leak rate of the gas cell was recorded for at least 0.5 h. The steady-state permeabilities of gas A, P_A , at five different upstream pressures (i.e., 30, 80, 130, 180, and 230 psig) in Barrer (1 Barrer = 10^{-10} cm³ (STP) cm/cm² s cm Hg) were determined from the downstream pressure as follows:

$$P_{\rm A} = \frac{V_{\rm d}l}{p_2 ART} \left[\left(\frac{{\rm d}p_1}{{\rm d}t} \right)_{\rm ss} - \left(\frac{{\rm d}p_1}{{\rm d}t} \right)_{\rm leak} \right]$$

where $V_{\rm d}$ is the fixed downstream volume of the gas cell in cm³, l is the experimentally measured membrane thickness in cm, p_2 is the absolute upstream pressure in cm Hg, $\left(\frac{{\rm d}p_1}{{\rm d}t}\right)_{\rm ss}$ and $\left(\frac{{\rm d}p_1}{{\rm d}t}\right)_{\rm leak}$ are pressure increases (cm Hg/s) in the fixed downstream volume at a fixed upstream pressure under steady-state and vacuum, respectively, A is the available membrane area in cm² for gas transport, R (R = 0.278 cm³ cm Hg/cm³ (STP)·K) is the gas constant, and T (308 K) is the setting temperature.

Pure gas permeabilities (H2 and CH4) of crosslinked films at high temperatures of up to 180 °C were measured in a broad pressure range (i.e., 30-130 psig). 30-32 The samples were prepared by masking the crosslinked films on to copper disk with a pre-punched hole using Master Bond EP46HT-2 epoxy at 100 °C, and the exposed area was measured on a scanner. The prepared sample was heated on a heating plate at 100 °C for 1 h to partially cure the epoxy and then loaded in the gas cell in an oven with controlled temperature and isotherm using predetermined procedures while degassing on both sides to completely cure the epoxy and prevent thermal oxidation at high temperatures. The heating procedure was set as 100, 120, 150, and 180 °C for 3 h at each stage to completely cure the epoxy glue, followed by an isotherm at 180 °C for another 6 h to eliminate the potential influence of moisture; then, the oven was naturally cooled down to the testing temperature. The sample was degassed and maintained at the isothermal testing

temperature overnight before testing. For each sample, H_2 and CH_4 were tested at 50, 100, 150, and 180 $^{\circ}C$ in sequence.

The permeability of polymers at varied temperatures is typically expressed by the Arrhenius—van't Hoff relationships: 33

$$P = P_0 e^{-E_p/RT}$$

where P_0 is the exponential prefactor and E_p is the permeation activation energy in kJ/mol.

The ideal selectivity, $\alpha_{A/B}$, where gas A is the more permeable gas, is determined as follows:⁸

$$\alpha_{A/B} = P_A / P_B$$

The diffusion coefficient, D, is calculated using the time-lag method from the experimentally measured film thickness l in cm and lag time θ in s:³⁴

$$D = \frac{l^2}{6\theta}$$

The solubility coefficient (*S*) values are then confirmed based on the solution-diffusion model:

$$P = D \times S$$

Correspondingly, the diffusivity selectivity ($\alpha_{D,A/B}$) and solubility selectivity ($\alpha_{S,A/B}$) are as follows:

$$\alpha_{\text{D,A/B}} = \frac{D_{\text{A}}}{D_{\text{B}}}, \quad \alpha_{\text{S,A/B}} = \frac{S_{\text{A}}}{S_{\text{B}}}$$

3. RESULTS AND DISCUSSION

3.1. Synthesis of the Telechelic Oligomer and Characterization. Phenylethynyl-terminated sPPBO oligomers with systematically varied molecular weights (4000–12 000 g/mol) were synthesized as described before. The chemical structures of the synthesized sPPBO oligomers and their linear control, LsPPBO, are confirmed by ¹H NMR. Full peak assignments for all of the oligomers and controls are provided in Figure S1. Figure 2 presents ¹H NMR spectra of representative sPPBO oligomers (4k and 8k) and the highmolecular-weight (MW) linear control. As shown, the peak intensity of phenylethynyl end groups (7.4-8.3 ppm) and -OH group (~7.1 ppm) at the chain ends (highlighted in dotted frames) increases with decreasing oligomer MW. The molecular weight of sPPBO oligomers is determined by the integration ratio of the end group peak (red arrow) and the peak that belongs to the bridgehead protons of pentiptycene units in the main chain (blue arrow). As summarized in Table S1, the actual numbers of repeating units (i.e., degree of polymerization) determined from the end group analysis agree with the target MW, demonstrating well-controlled MW and completion of end-capping of both ends of sPPBO oligomers.

DSC experiments were performed to determine the thermal treatment protocols for thermal end-linking and membrane preparation. According to the chemical structure of sPPBO oligomers, two thermally driven reactions may occur at the chain ends upon heating (Scheme 2): exothermic crosslinking of phenylethynyl groups and endothermic thermal rearrangement (TR) between the imide carbonyl group and the adjacent *ortho*-hydroxyl group to form benzoxazole structures. As shown in Figure 3, the endothermic TR process of the oligomer starts at around 270–320 °C (depending on the oligomer MW) and

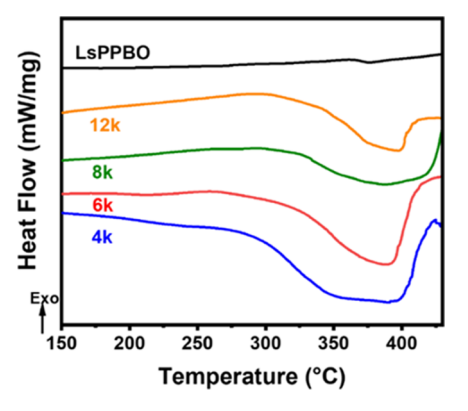


Figure 3. DSC analysis (second heating cycle) of sPPBO oligomers and the linear control, LsPPBO.

the exothermic crosslinking of the phenylethynyl group occurs at about 375–400 °C. In addition, the relative heat flows of both crosslinking and TR decay with increasing oligomer MW because of a reduced content of functional end groups. It is noticed that long oligomers with a higher starting TR temperature due to more restricted mobility showed an overlapped temperature range of the TR process and thermal crosslinking. Based on DSC results, the thermal protocol for the preparation of crosslinked unimodal network membranes is established as follows: 10 °C/min to 180 °C followed by 4 °C/min to 300 °C (Ramp I); a 2 h isothermal annealing at 300 °C to facilitate segmental motion for efficient TR process (Isotherm I); 50 °C/min to 400 °C (Ramp II); 1 h isothermal treatment at 400 °C to complete crosslinking (Isotherm II); and a final natural cooling process (cooling).

The thermal stability of sPPBO oligomers and LsPPBO was assessed by TGA analysis (Figure S2). While LsPPBO shows a typical single-stage weight-loss profile with excellent thermal stability ($T_{d,5\%} > 500$ °C), all of the fully dried oligomers except the 4k oligomer exhibit a two-stage weight-loss profile (Figure S2). The 4k oligomer, i.e., the shortest oligomer, shows a three-stage weight loss profile, where the early weight loss around 270 °C is likely induced by the degradation of very short chains. Consistent with the endothermic TR process peaks observed in DSC, the first-stage (second-stage for 4k oligomer) weight loss can be ascribed to the TR process.³⁵ This is also evidenced by the observation that the first-stage weight loss decreases with increasing MW due to a reduced amount of TR-able functional groups near the chain ends. In all cases, the onset of the second-stage weight loss exceeds 500 °C, indicating excellent thermal stability of the crosslinked sPPBO structures.

3.2. Thermal End-Linking and Membrane Characterization. A series of crosslinked unimodal network membranes, with a systematically varied crosslink density as described by the inter-crosslink chain length (i.e., U4k, U6k, U8k, and U12k), was prepared using the predetermined thermal protocol as described above. No weight loss was detected after the crosslinked membranes were immersed in hot NMP for a week, demonstrating the completion of crosslinking in all of the crosslinked membranes, i.e., 100% gel fraction, using the established thermal protocols. Thermal stabilities of crosslinked membranes were studied by TGA and DSC. No glass transition temperature (T_g) was detected for all of the crosslinked membranes due to highly restricted segmental motion in these fully crosslinked membranes. As displayed in

Figure S4, all of the crosslinked membranes present a singlestage decomposition at above 500 °C. The chemical structure of crosslinked sPPBO films were confirmed by ATR-FTIR from the disappearance (e.g., $-C \equiv C-$, imide -C=O) and appearance (e.g., benzoxazole) of characteristic peaks before and after the crosslinking and TR process. As shown in Figure S5, the characteristic benzoxazole bands of sPPBO oligomers, i.e., 1562 cm⁻¹ (C=N) and 1048 cm⁻¹ (C-O), are wellpreserved, indicating well-maintained polybenzoxazole backbones in the crosslinked membranes. Comparing the 4k oligomer and U4k membrane, the $-C \equiv C - \text{peak} (2160 \text{ cm}^{-1})$ of the phenylethynyl end groups disappears in the crosslinked U4k film, suggesting the formation of fully crosslinked network structures.^{35–37} A weak C=C band was detected at 1660 cm⁻¹, implying an ethynyl-ethynyl addition during crosslinking, which yields polyenes with alternating single and double bonds at curing junctions as a hypothetical structure shown in Scheme S1. In addition, the imide bands near the end groups, i.e., C-N and C-N-C adsorption at 1367 and 1105 cm⁻¹, vanish completely after thermal treatment as expected, although the trace amount of the C=O stretching peak may suggest the suppressed thermal conversion because of the construction of rigid crosslinked networks that may impede the TR process due to a lack of segmental mobility for the solidstate TR conversion as demonstrated in previous re-

WAXS was conducted to estimate the interchain distance and chain packing in the crosslinked membranes. As presented (Figure S6), three broad halos (labeled as A, B, and C) confirm amorphous structures of the crosslinked and linear membranes. Table 1 summarizes the calculated *d*-spacing values for all of

Table 1. Interchain *d*-Spacing by WAXS, Density, and Fraction of Free Volume (FFV) of Crosslinked and Linear sPPBO Films

			d-spacing (Å)		
film	density (g/cm³)	FFV (%)	A	В	С
U4k	1.308 ± 0.005	16.8 ± 0.3	9.1	5.5	3.7
U6k	1.305 ± 0.004	17.7 ± 0.2	9.4	5.4	3.8
U8k	1.306 ± 0.007	18.5 ± 0.4	9.5	5.3	3.9
U12k	1.275 ± 0.009	21.2 ± 0.5	9.5	5.3	3.7
LsPPBO	1.284 ± 0.005	24.3 ± 0.3	9.6	5.3	3.8

the membranes. Specifically, peak A positioned at ~4.7° (dspacing of ~9 Å) likely correlates to the general amorphous packing of the bulky pentiptycene-containing segments, peak B at $\sim 8^{\circ}$ (d-spacing of ~ 5 Å) may correspond to the domain of the chain segments without the bulky pentiptycene unit, and the weak shoulder at $\sim 23^{\circ}$ (d-spacing of ~ 3.8 Å) can be ascribed to the π - π stacking between aromatic rings of pentiptycene moieties as reported in previous reports.4 Compared with the linear film, crosslinked films exhibit a stronger peak intensity, suggesting likely more regulated segmental packing due to the formation of unimodal network structures. As shown in Table 1, d-spacing values of peaks A and B show opposite trends as a function of the crosslink density, signifying the competing effects of TR conversion (generally increased *d*-spacing due to benzoxazole formation) and crosslinking (generally decreased d-spacing due to densification). As the crosslinked density decreases from U4k to U12k, the calculated d-spacing values of peak A increase from 9.1 to 9.5 Å, while the *d*-spacing values of peak B decrease from 5.5 to 5.3 Å. These results seem to suggest that at a high crosslink density (e.g., U4k), the crosslinking-induced densification effect is dominant, which leads to a much lower d-spacing value for peak A in U4k than those of other crosslinked membranes and the linear control. Similar observations of crosslinking-induced densification have been widely made in crosslinked glassy polymers such as polyimides. 40,41,44,45 The slightly higher d-spacing values of peak B in more densely crosslinked membranes likely result from the formation of benzoxazole structures from the TR conversion along with the presence of bulky phenyl groups from the end-linking process at the crosslink sites, which compensate the crosslinking-induced densification effect as more densely crosslinked membranes have a higher fraction of crosslink sites. The FFV of the crosslinked and linear films was calculated from the measured density data. To simplify the calculations, the ethynyl end groups were assumed to be fully converted to C=C according to the FTIR and gel fraction data. As tabulated in Table 1, the FFV of the crosslinked films generally increases as the crosslink density decreases and is lower than the linear control as expected.

3.3. Gas Permeation and Structure–Property Relationships. Pure-gas permeation tests of the fresh membranes were measured between 2 and 16 atm for five gases in the order of H₂, CH₄, N₂, O₂, and CO₂. The obtained permeability and calculated ideal selectivity of fresh films are tabulated in Table S3. The single-gas permeability of all of the films aligns

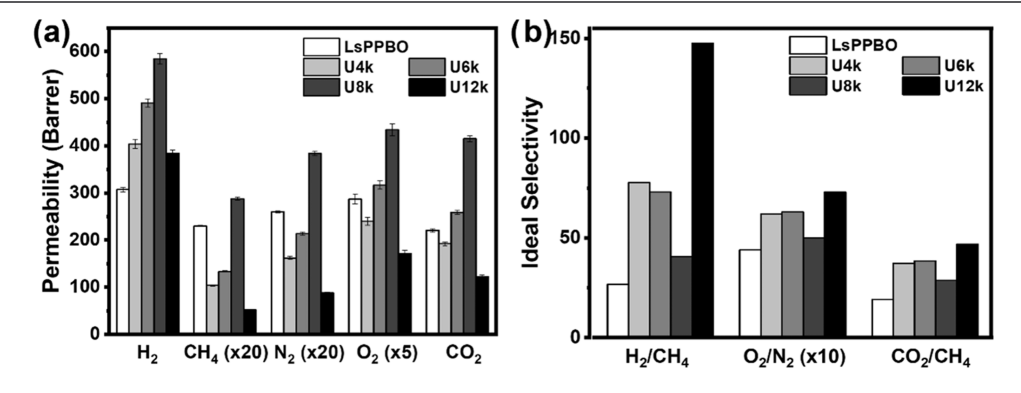


Figure 4. (a) Permeability and (b) ideal selectivity of the crosslinked and linear LsPPBO membranes (note: for better visual effect, the permeability values of CH_4 , N_2 , and O_2 are multiplied by 20, 20, and 5, respectively, and the O_2/N_2 selectivity is multiplied by 10, as marked in the permeability and ideal selectivity plot).

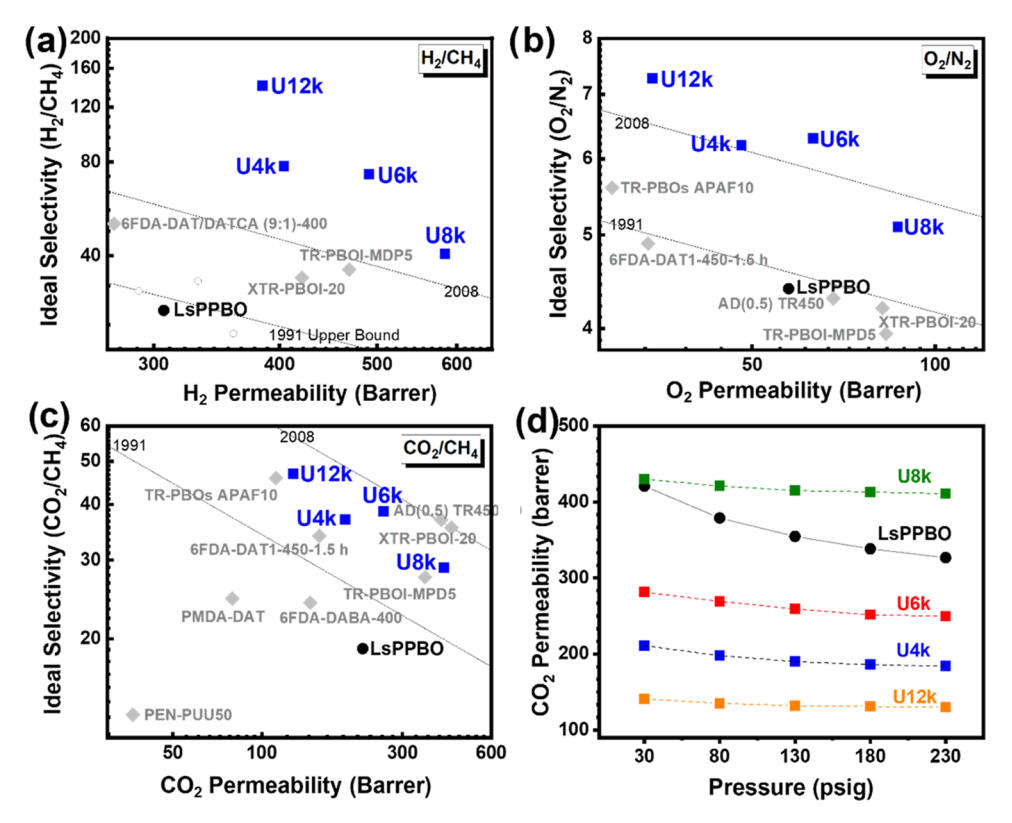


Figure 5. Benchmarking separation performance of crosslinked sPPBO membranes against the upper bounds for (a) H_2/CH_4 , (b) O_2/N_2 , and (c) CO_2/CH_4 , and (d) pressure dependence of CO_2 permeation at 35 °C for crosslinked films and linear LsPPBO. Data points of randomly crosslinked PBO (gray diamonds) for comparisons: TR-PBOI-MPD5, ⁴⁶ XTR-PBOI-25, ⁴⁷ TR-PBOs APAF10, ⁴⁸ AD (0.5) TR450, ⁴⁹ 6FDA-DAT1-450-1.5h, ¹¹ 6FDA-DABA-400, ⁵⁰ PMDA-DAT, ⁵¹ PEN-PU 50, ⁵² and 6FDA-DAT/DATCA (9:1)-400. ⁵³

in the order of kinetic diameters of gas molecules (i.e., $P_{\rm CH_4}$ < $P_{\rm N_2}$ < $P_{\rm O_2}$ < $P_{\rm CO_2}$ < $P_{\rm H_2}$), signifying the size-sieving mechanism. Compared with the uncrosslinked linear control (LsPPBO), all of the crosslinked unimodal networks exhibit significant enhancement in permeability and/or selectivity depending on the crosslink density. The much-enhanced separation performance of crosslinked membranes indicates that the model network structures formed by concurrent TR conversion and end-linking effectively counteract the effect of crosslinking-induced densification frequently seen in randomly crosslinked membranes due to the excess free volume with desired size-sieving properties enabled through the formation of a benzoxazole structure and bulky phenyl groups at the crosslink sites.

Figure 4 compares the permeability and ideal selectivity of crosslinked membranes with the linear control to reveal the influence of the crosslink density on gas transport. Fundamental analysis of diffusivity and solubility coefficients along with diffusivity and solubility selectivity as a function of the crosslink density is plotted in Figure S7. Compared with the uncrosslinked linear counterpart, all of the crosslinked membranes present higher H₂ permeability regardless of the crosslink density, signifying the formation of ultraporous structures in the crosslinked unimodal sPPBO membranes. The permeability of all other gases, however, shows strong dependence on the crosslink density due to the interplay of TR conversion and thermal end-linking. Generally, in randomly crosslinked membranes, a high crosslink density leads to low gas permeability due to crosslinking-induced compact chain packing in the crosslinked membranes. However, as shown in

Figure 4a, crosslinked sPPBO model networks show a nonlinear relationship between permeability and the crosslink density, where gas permeability increases as the crosslink density decreases from U4k to U8k as expected, but then exhibits a marked decrease in the most loosely crosslinked membrane, i.e., U12k. This trend can be rationalized by the compact segmental packing of long chains (12k) along with a low content of bulky end-groups at a low crosslink density, which agrees well with the decreased interchain distance at a decreased crosslink density as observed in WAXS. Correspondingly, diffusivity coefficients (D) shown in Figure S7a show an initial increase in diffusivity with decreasing crosslink density followed by a decreasing trend in more loosely crosslinked membranes because of tighter segmental packing of longer chains upon thermal treatment. This is also consistent with the observation that the diffusivity coefficients of the U12k membrane with the longest inter-crosslink chain length are very comparable to the linear control for all of the gases tested. On the other hand, the effect of the crosslink density on the solubility coefficient (S) seems to be significant only for condensable gases such as CO2 as all the crosslinked membranes show comparable O2 and CH4 solubility coefficients (Figure S7b). The suppressed solubility coefficients of crosslinked networks with a high crosslink density (i.e., U4k and U6k) are likely due to greatly reduced sorption sites in densely crosslinked networks relative to the linear control. The much-increased solubility coefficient of U8k is likely induced by the presence of a benzoxazole structure and phenyl rings at the curing joints, which enhance the interaction with CO₂ molecules and counteract the densification effect.⁴¹ Similar to diffusivity coefficients, the solubility coefficients of

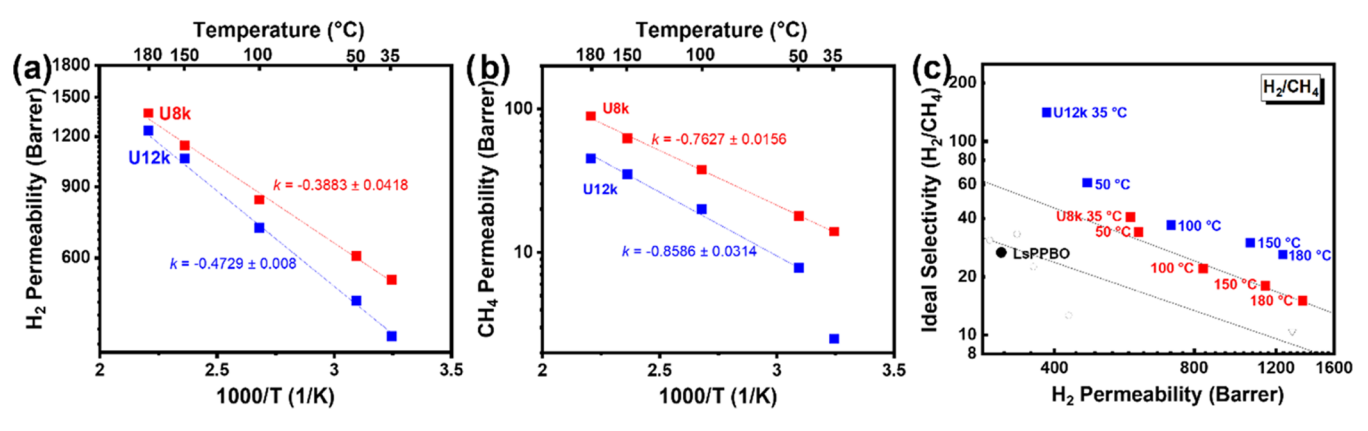


Figure 6. (a) Temperature dependence of H₂; (b) temperature dependence of CH₄; and (c) gas separation performance of crosslinked films and controls against the permeability/selectivity trade-off for H₂/CH₄. All data reported in this figure are at a feed pressure of 130 psig.

U12k approximates the linear control LsPPBO due to its long inter-crosslink chain length.

Figure 4b presents the ideal selectivity of crosslinked unimodal networks compared with the linear control LsPPBO. As a result of the greatly enhanced permeability of small gas molecules (e.g., H₂) and suppressed transport of large gases (CH₄), all of the crosslinked membranes display much more attractive ideal selectivity for H₂/CH₄, O₂/N₂, and CO₂/CH₄ separations than the linear control, demonstrating the greatly enhanced size-sieving ability by constructing crosslinked model networks via thermal end-linking. Among the crosslinked membranes, a similar nonlinear relationship between the ideal selectivity and the crosslink density is observed. The ideal selectivity initially decreases slightly with a decreasing crosslink density (or increasing inter-crosslink chain length) as expected and then exhibits an increase in the U12k membrane that has the longest inter-crosslink chain length. Analysis of the respective contribution from diffusivity selectivity and solubility selectivity (Figure S7c,d) suggests that the separation efficiency is dominated by the diffusivity selectivity for most gas pairs, which shows the same trend as the overall ideal

Figure 5a—c plots the crosslinked films and the linear control against the upper bounds for various gas pairs. Regardless of the crosslink density, the separation performance of all of the crosslinked membranes greatly outperforms the linear LsPPBO membrane, signifying the significance of the controlled endlinking approach that is unparalleled by random crosslinking where randomly crosslinked membranes typically show a deteriorated separation performance as compared with their linear counterparts. In addition, the broad range of superior separation performance displayed by these model networks that is tailored via precise control of the crosslink density affects the excellent tunability of the model network design involving controlled end-linking of telechelic oligomers. Examination of the pressure dependence of CO₂ permeability (Figure 5d) shows that all of the crosslinked sPPBO network membranes display very stable permeability at increasing CO₂ pressure compared with LsPPBO, demonstrating their potential of improved resistance to CO₂ plasticization, which will be investigated further via mixed-gas permeation tests.

3.4. High-Temperature H₂/CH₄ Permeation. Membranes that are thermally stable as well as able to main high separation performance at elevated temperatures are highly desirable as they facilitate the integration of membrane separation with high-temperature catalysis processes, eliminat-

ing or reducing repeated energy-intensive cooling—heating cycles.^{2,3} However, polymeric membranes, even with sufficient thermal stability, lose their size-sieving property at elevated temperatures due to thermally expanded gas diffusion pathways allowing for all gases to pass through. These challenges account for the very limited high-temperature permeation data for existing polymers besides polybenzox-azoles (PBI) for H₂/CO₂ separation. Because of the superior thermal stability and stable microstructure enabled by chemical crosslinking, our crosslinked membranes may be well-suited for high-temperature gas separation applications.

Among the crosslinked films, the most selective film, U12k, and the most permeable film, U8k, were examined in temperature-dependence studies for H₂/CH₄ separations. As shown in Figure 6, H2 permeability increases proportionally to temperature following the Arrhenius relationship, demonstrating diffusion-controlled gas transport mechanisms within the temperature range examined in this study. The temperature dependence of permeability was evaluated by the activation energy (E_p) , wherein the E_p (kJ/mol) was calculated from Arrhenius relationship from the slope (k) of the fitting equation $\left(\frac{E_p}{R} = -\frac{\partial \ln P}{\partial 1 / T}\right)$. Consistent with the size-sieving mechanism, the large gas CH4 shows a much stronger temperature dependence than small gas H₂ due to its high activation energy. Compared with the permeability measured under ambient conditions, the increased CH₄ permeability of U12k at high temperatures likely induced the thermal annealing during sample preparation as large gas molecules are more sensitive to the microstructure, whereas the U8k with a higher crosslink density shows improved linearity.

The permeability and selectivity of U8k and U12k between 35 and 180 °C were plotted against the upper bound and compared with the linear control LsPPBO (Figure 6). As the temperature increases from 35 to 180 °C, both H₂ and CH₄ permeabilities increase with declined selectivity as expected due to the faster increase in CH₄ permeability with temperature. However, the gain in H₂ permeability outweighs the loss of H₂/CH₄ selectivity with increasing temperature, resulting in the overall separation performance remaining above the upper bound for the entire temperature range up to 180 °C. These exciting results suggest that the construction of well-defined crosslinked model network structures has great potential to enable the use of polymeric membranes for efficient gas separation at elevated temperatures.

4. CONCLUSIONS

The chemical structure and the oligomer MW (i.e., 4k, 6k, 8k, 12k) were confirmed by ¹H NMMR. Pentiptycene-based crosslinked unimodal network membranes with a finely tailored crosslink density, represented by the inter-crosslink chain length (i.e., U4k, U6k, U8k, and U12k), were prepared via the thermal end-linking method from phenylethynylterminated pentiptycene-based telechelic polybenzoxazole oligomers of controlled molecular weight (MW) ranging from 4000 to 12 000 g/mol. The completion of crosslinking and superior thermal stability were confirmed by gel fraction measurements, FTIR, and TGA analysis. FFV and WAXS analyses show a nonlinear relationship with the crosslink density, which is ascribed to the competing effects between crosslinking-induced densification and the formation of bulky benzoxazole and phenyl groups at the crosslink sites. Pure-gas permeation tests under ambient conditions demonstrate concurrent improvements in the selectivity and permeability of crosslinked membranes over their linear control. The effect of the crosslink density is consistent with the microstructure analysis among the crosslinked membranes. The wellmaintained H₂/CH₄ separation performance at high temperatures up to 180 °C further extend this study for hightemperature applications. The outstanding separation performance of crosslinked unimodal networks demonstrates the novelty of the model network design that is unparalleled by random crosslinking methods and provides a fundamentally new dimension in the design of high-performance crosslinked membranes for gas separations under harsh conditions.

ASSOCIATED CONTENT

Supporting Information

The Supporting Information is available free of charge at https://pubs.acs.org/doi/10.1021/acs.chemmater.2c02143.

Detailed information on ¹H NMR spectra of sPPBO oligomers and the high-molecular-weight linear polymer; stoichiometry control of reactants for the synthesis of sPPBO oligomers and MW confirmation; scheme of the theoretical crosslink and thermal rearrangement reaction; TGA and TGA derivative weight loss of sPPBO oligomers and the LsPPBO polymer; TGA profile of oligomers and the high-MW polymer by a predetermined thermal protocol; TGA profile of the crosslinked sPPBO film and LsPPBO; crosslinked membranes and LsPPBO thermal properties; FTIR spectra of oligomers, crosslinked films, and LsPPBO; WAXS profile of crosslinked sPPBO and linear LsPPBO films; pure gas diffusivity coefficients, solubility coefficients, diffusivity selectivity, and solubility selectivity of the crosslinked and linear LsPPBO membranes; pure-gas separation performance of the crosslinked sPPBO and LsPPBO films at 35 °C; pure-gas diffusivity coefficients, solubility coefficients, diffusivity selectivity, and solubility selectivity of the crosslinked sPPBO and LsPPBO films at 35 °C, and GPC of 4k sPPBO (PDF)

AUTHOR INFORMATION

Corresponding Author

Ruilan Guo – Department of Chemical and Biomolecular Engineering, University of Notre Dame, Notre Dame, Indiana 46556, United States; ⊚ orcid.org/0000-0002-3373-2588;

Phone: +1-574-631-3453; Email: rguo@nd.edu; Fax: +1-574-631-8366

Authors

- Si Li Department of Chemical and Biomolecular Engineering, University of Notre Dame, Notre Dame, Indiana 46556, United States
- Ziwei Dai Department of Chemical and Biomolecular Engineering, University of Notre Dame, Notre Dame, Indiana 46556, United States
- Tao Wang Department of Chemical and Biomolecular Engineering, University of Notre Dame, Notre Dame, Indiana 46556, United States
- Zihan Huang Department of Chemical and Biomolecular Engineering, University of Notre Dame, Notre Dame, Indiana 46556, United States

Complete contact information is available at: https://pubs.acs.org/10.1021/acs.chemmater.2c02143

Author Contributions

This manuscript was written through contributions of all authors. All authors have given approval to the final version of the manuscript.

Notes

The authors declare no competing financial interest.

ACKNOWLEDGMENTS

This study is supported by the National Science Foundation under Cooperative Agreement No. EEC-1647722. Any opinions, findings, and conclusions or recommendations expressed in this material are those of the author(s) and do not necessarily reflect the views of the National Science Foundation. The authors thank the Center for Environmental Science and Technology (CEST) of the University of Notre Dame for the use of characterization facilities.

■ REFERENCES

- (1) Baker, R. W. Future Directions of Membrane Gas Separation Technology. *Ind. Eng. Chem. Res.* **2002**, *41*, 1393–1411.
- (2) Bernardo, P.; Drioli, E.; Golemme, G. Membrane Gas Separation: A Review/State of the Art. *Ind. Eng. Chem. Res.* **2009**, 48, 4638–4663.
- (3) Koros, W. J.; Mahajan, R. Pushing the Limits on Possibilities for Large Scale Gas Separation: Which Strategies? *J. Membr. Sci.* **2001**, 181, 141.
- (4) Robeson, L. M. The Upper Bound Revisited. *J. Membr. Sci.* **2008**, 320, 390–400.
- (5) Robeson, L. M. Correlation of Separation Factor versus Permeability for Polymeric Membranes. *J. Membr. Sci.* **1991**, *62*, 165–185
- (6) Robeson, L. M.; Liu, Q.; Freeman, B. D.; Paul, D. R. Comparison of Transport Properties of Rubbery and Glassy Polymers and the Relevance to the Upper Bound Relationship. *J. Membr. Sci.* **2015**, 476, 421–431.
- (7) Comesaña-Gándara, B.; Chen, J.; Bezzu, C. G.; Carta, M.; Rose, I.; Ferrari, M. C.; Esposito, E.; Fuoco, A.; Jansen, J. C.; McKeown, N. B. Redefining the Robeson Upper Bounds for CO_2/CH_4 and CO_2/N_2 Separations Using a Series of Ultrapermeable Benzotriptycene-Based Polymers of Intrinsic Microporosity. *Energy Environ. Sci.* **2019**, *12*, 2733–2740.
- (8) Sanders, D. F.; Smith, Z. P.; Guo, R.; Robeson, L. M.; McGrath, J. E.; Paul, D. R.; Freeman, B. D. Energy-Efficient Polymeric Gas Separation Membranes for a Sustainable Future: A Review. *Polymer* **2013**, *54*, 4729–4761.

- (9) Koros, W. J.; Zhang, C. Materials for Next-Generation Molecularly Selective Synthetic Membranes. *Nat. Mater.* **2017**, *16*, 289–297.
- (10) Lee, W. H.; Seong, J. G.; Bae, J. Y.; Wang, H. H.; Moon, S. J.; Jung, J. T.; Do, Y. S.; Kang, H.; Park, C. H.; Lee, Y. M. Thermally Rearranged Semi-Interpenetrating Polymer Network (TR-SIPN) Membranes for Gas and Olefin/Paraffin Separation. *J. Membr. Sci.* **2021**, *625*, No. 119157.
- (11) Yerzhankyzy, A.; Wang, Y.; Ghanem, B. S.; Puspasari, T.; Pinnau, I. Gas Separation Performance of Solid-State in-Situ Thermally Crosslinked 6FDA-Based Polyimides. *J. Membr. Sci.* **2022**, *641*, No. 119885.
- (12) Yu, H. J.; Chan, C. H.; Nam, S. Y.; Kim, S. J.; Yoo, J. S.; Lee, J. S. Thermally Cross-Linked Ultra-Robust Membranes for Plasticization Resistance and Permeation Enhancement A Combined Theoretical and Experimental Study. *J. Membr. Sci.* **2022**, *646*, No. 120250.
- (13) Xu, S.; Ren, X.; Zhao, N.; Wu, L.; Zhang, Z.; Fan, Y.; Li, N. Self-Crosslinking of Bromomethylated 6FDA-DAM Polyimide for Gas Separations. *J. Membr. Sci.* **2021**, *636*, No. 119534.
- (14) Wind, J. D.; Staudt-Bickel, C.; Paul, D. R.; Koros, W. J. The Effects of Crosslinking Chemistry on CO₂ Plasticization of Polyimide Gas Separation Membranes. *Ind. Eng. Chem. Res.* **2002**, *41*, 6139–6148.
- (15) Lin, H.; Kai, T.; Freeman, B. D.; Kalakkunnath, S.; Kalika, D. S. The Effect of Cross-Linking on Gas Permeability in Cross-Linked Poly(Ethylene Glycol Diacrylate). *Macromolecules* **2005**, *38*, 8381–8393
- (16) Liu, Y.; Wang, R.; Chung, T. S. Chemical Cross-Linking Modification of Polyimide Membranes for Gas Separation. *J. Membr. Sci.* **2001**, *189*, 231–239.
- (17) Hirayama, Y.; Kase, Y.; Tanihara, N.; Sumiyama, Y.; Kusuki, Y.; Haraya, K. Permeation Properties to CO₂ and N₂ of Poly(Ethylene Oxide)-Containing and Crosslinked Polymer Films. *J. Membr. Sci.* **1999**, *160*, 87–99.
- (18) Berean, K.; Ou, J. Z.; Nour, M.; Latham, K.; McSweeney, C.; Paull, D.; Halim, A.; Kentish, S.; Doherty, C. M.; Hill, A. J.; Kalantar-Zadeh, K. The Effect of Crosslinking Temperature on the Permeability of PDMS Membranes: Evidence of Extraordinary CO₂ and CH₄ Gas Permeation. Sep. Purif. Technol. **2014**, 122, 96–104.
- (19) Isfahani, A. P.; Ghalei, B.; Wakimoto, K.; Bagheri, R.; Sivaniah, E.; Sadeghi, M. Plasticization Resistant Crosslinked Polyurethane Gas Separation Membranes. *J. Mater. Chem. A* **2016**, *4*, 17431–17439.
- (20) Kwisnek, L.; Heinz, S.; Wiggins, J. S.; Nazarenko, S. Multifunctional Thiols as Additives in UV-Cured PEG-Diacrylate Membranes for CO₂ Separation. *J. Membr. Sci.* **2011**, *369*, 429–436.
- (21) Lin, H.; Wagner, E.; van Swinnea, J. S.; Freeman, B. D.; Pas, S. J.; Hill, A. J.; Kalakkunnath, S.; Kalika, D. S. Transport and Structural Characteristics of Crosslinked Poly(Ethylene Oxide) Rubbers. *J. Membr. Sci.* **2006**, 276, 145–161.
- (22) Kline, G. K.; Weidman, J. R.; Zhang, Q.; Guo, R. Studies of the Synergistic Effects of Crosslink Density and Crosslink Inhomogeneity on Crosslinked PEO Membranes for CO₂-Selective Separations. *J. Membr. Sci.* **2017**, *544*, 25–34.
- (23) Kline, G. K.; Zhang, Q.; Weidman, J. R.; Guo, R. PEO-Rich Semi-Interpenetrating Polymer Network (s-IPN) Membranes for CO₂ Separation. *J. Membr. Sci.* **2017**, *544*, 143–150.
- (24) Li, S.; McGinness, H.; Wang, T.; Guo, R. Crosslinked Matrimid-like Polyimide Membranes with Unimodal Network Structure for Enhanced Stability and Gas Separation Performance. *Polymer* **2021**, 237, No. 124323.
- (25) Huang, Z.; Yin, C.; Corrado, T.; Li, S.; Zhang, Q.; Guo, R. Microporous Pentiptycene-Based Polymers with Heterocyclic Rings for High-Performance Gas Separation Membranes. *Chem. Mater.* **2022**, *34*, 2730–2742.
- (26) Fang, X.; Xie, X. Q.; Simone, C. D.; Stevens, M. P.; Scola, D. A. Solid-State 13C NMR Study of the Cure of ¹³C-Labeled Phenylethynyl End-Capped Polyimides. *Macromolecules* **2000**, 33, 1671–1681.

- (27) Luo, S.; Liu, Q.; Zhang, B.; Wiegand, J. R.; Freeman, B. D.; Guo, R. Pentiptycene-Based Polyimides with Hierarchically Controlled Molecular Cavity Architecture for Efficient Membrane Gas Separation. *J. Membr. Sci.* **2015**, *480*, 20–30.
- (28) Luo, S.; Liu, J.; Lin, H.; Kazanowska, B. A.; Hunckler, M. D.; Roeder, R. K.; Guo, R. Preparation and Gas Transport Properties of Triptycene-Containing Polybenzoxazole (PBO)-Based Polymers Derived from Thermal Rearrangement (TR) and Thermal Cyclodehydration (TC) Processes. *J. Mater. Chem. A* **2016**, *4*, 17050–17062.
- (29) Xiao, Y.; Zhang, L.; Xu, L.; Chung, T. S. Molecular Design of Tröger's Base-Based Polymers with Intrinsic Microporosity for Gas Separation. *J. Membr. Sci.* **2017**, *521*, 65–72.
- (30) Omidvar, M.; Stafford, C. M.; Lin, H. Thermally Stable Cross-Linked P84 with Superior Membrane H₂/CO₂ Separation Properties at 100 °C. *J. Membr. Sci.* **2019**, *575*, 118–125.
- (31) Omidvar, M.; Nguyen, H.; Liang, H.; Doherty, C. M.; Hill, A. J.; Stafford, C. M.; Feng, X.; Swihart, M. T.; Lin, H. Unexpectedly Strong Size-Sieving Ability in Carbonized Polybenzimidazole for Membrane H₂/CO₂ Separation. *ACS Appl. Mater. Interfaces* **2019**, *11*, 47365–47372.
- (32) Borjigin, H.; Stevens, K. A.; Liu, R.; Moon, J. D.; Shaver, A. T.; Swinnea, S.; Freeman, B. D.; Riffle, J. S.; McGrath, J. E. Synthesis and Characterization of Polybenzimidazoles Derived from Tetraaminodiphenylsulfone for High Temperature Gas Separation Membranes. *Polymer* **2015**, *71*, 135–142.
- (33) Ghosal, K.; Freeman, B. D. Gas Separation Using Polymer Membranes: An Overview. *Polym. Adv. Technol.* **1994**, *5*, 673–697.
- (34) Weidman, J. R.; Luo, S.; Breier, J. M.; Buckley, P.; Gao, P.; Guo, R. Triptycene-Based Copolyimides with Tailored Backbone Rigidity for Enhanced Gas Transport. *Polymer* **2017**, *126*, 314–323.
- (35) Yue, J.; Li, Y.; Zhao, Y.; Xiang, D.; Dai, Y. Thermal Degradation Behavior of Carborane-Containing Phenylethynyl Terminated Imide Systems. *Polym. Degrad. Stab.* **2016**, *129*, 286–295.
- (36) Cho, D.; Drzal, L. T. Characterization, Properties, and Processing of LaRCTM PETI-5 as a High-Temperature Sizing Material. I. FTIR Studies on Imidization and Phenylethynyl End-Group Reaction Behavior. J. Appl. Polym. Sci. 2000, 76, 190–200.
- (37) Li, Y.; Morgan, R. J. Thermal Cure of Phenylethynyl-Terminated AFR-PEPA-4 Imide Oligomer and a Model Compound. *J. Appl. Polym. Sci.* **2006**, *101*, 4446–4453.
- (38) Guo, R.; Sanders, D. F.; Smith, Z. P.; Freeman, B. D.; Paul, D. R.; McGrath, J. E. Synthesis and Characterization of Thermally Rearranged (TR) Polymers: Influence of Ortho-Positioned Functional Groups of Polyimide Precursors on TR Process and Gas Transport Properties. J. Mater. Chem. A 2013, 1, 262–272.
- (39) Han, S. H.; Misdan, N.; Kim, S.; Doherty, C. M.; Hill, A. J.; Lee, Y. M. Thermally Rearranged (TR) Polybenzoxazole: Effects of Diverse Imidization Routes on Physical Properties and Gas Transport Behaviors. *Macromolecules* **2010**, *43*, 7657–7667.
- (40) Swaidan, R.; Ghanem, B.; Litwiller, E.; Pinnau, I. Effects of Hydroxyl-Functionalization and Sub-Tg Thermal Annealing on High Pressure Pure- and Mixed-Gas CO₂/CH₄ Separation by Polyimide Membranes Based on 6FDA and Triptycene-Containing Dianhydrides. *J. Membr. Sci.* **2015**, 475, 571–581.
- (41) Zhang, Q.; Luo, S.; Weidman, J.; Guo, R. Surface Modification of ZIF -90 with Triptycene for Enhanced Interfacial Interaction in Mixed-matrix Membranes for Gas Separation. *J. Polym. Sci.* **2020**, *58*, 2675–2687.
- (42) Corrado, T. J.; Huang, Z.; Huang, D.; Wamble, N.; Luo, T.; Guo, R. Pentiptycene-Based Ladder Polymers with Configurational Free Volume for Enhanced Gas Separation Performance and Physical Aging Resistance. *Proc. Natl. Acad. Sci. U.S.A.* **2021**, *118*, No. e2022204118.
- (43) Luo, S.; Zhang, Q.; Zhang, Y.; Weaver, K. P.; Phillip, W. A.; Guo, R. Facile Synthesis of a Pentiptycene-Based Highly Microporous Organic Polymer for Gas Storage and Water Treatment. ACS Appl. Mater. Interfaces 2018, 10, 15174–15182.

- (44) Chung, T. S.; Chng, M. L.; Pramoda, K. P.; Xiao, Y. PAMAM Dendrimer-Induced Cross-Linking Modification of Polyimide Membranes. *Langmuir* **2004**, *20*, 2966–2969.
- (45) Aziz, F.; Ismail, A. F. Preparation and Characterization of Cross-Linked Matrimid Membranes Using Para-Phenylenediamine for O_2/N_2 Separation. Sep. Purif. Technol. **2010**, 73, 421–428.
- (46) Calle, M.; Jo, H. J.; Doherty, C. M.; Hill, A. J.; Lee, Y. M. Cross-Linked Thermally Rearranged Poly(Benzoxazole-Co-Imide) Membranes Prepared from Ortho-Hydroxycopolyimides Containing Pendant Carboxyl Groups and Gas Separation Properties. *Macromolecules* **2015**, *48*, 2603–2613.
- (47) Calle, M.; Doherty, C. M.; Hill, A. J.; Lee, Y. M. Cross-Linked Thermally Rearranged Poly(Benzoxazole-Co-Imide) Membranes for Gas Separation. *Macromolecules* **2013**, *46*, 8179–8189.
- (48) Jo, H. J.; Soo, C. Y.; Dong, G.; Do, Y. S.; Wang, H. H.; Lee, M. J.; Quay, J. R.; Murphy, M. K.; Lee, Y. M. Thermally Rearranged Poly(Benzoxazole- Co -Imide) Membranes with Superior Mechanical Strength for Gas Separation Obtained by Tuning Chain Rigidity. *Macromolecules* **2015**, 48, 2194–2202.
- (49) Aguilar-Lugo, C.; Álvarez, C.; Lee, Y. M.; de La Campa, J. G.; Lozano, Á. E. Thermally Rearranged Polybenzoxazoles Containing Bulky Adamantyl Groups from Ortho-Substituted Precursor Copolyimides. *Macromolecules* **2018**, *51*, 1605–1619.
- (50) Thür, R.; Lemmens, V.; van Havere, D.; van Essen, M.; Nijmeijer, K.; Vankelecom, I. F. J. Tuning 6FDA-DABA Membrane Performance for CO₂ Removal by Physical Densification and Decarboxylation Cross-Linking during Simple Thermal Treatment. *J. Membr. Sci.* **2020**, *610*, No. 118195.
- (51) Li, F.; Zhang, C.; Weng, Y. Preparation and Gas Separation Properties of Triptycene-Based Microporous Polyimide. *Macromol. Chem. Phys.* **2019**, 220, No. 1900047.
- (52) Isfahani, A. P.; Sadeghi, M.; Wakimoto, K.; Shrestha, B. B.; Bagheri, R.; Sivaniah, E.; Ghalei, B. Pentiptycene-Based Polyurethane with Enhanced Mechanical Properties and CO₂-Plasticization Resistance for Thin Film Gas Separation Membranes. *ACS Appl. Mater. Interfaces* **2018**, *10*, 17366–17374.
- (53) Tian, Z.; Cao, B.; Li, P. Effects of Sub-Tg Cross-Linking of Triptycene-Based Polyimides on Gas Permeation, Plasticization Resistance and Physical Aging Properties. *J. Membr. Sci.* **2018**, *560*, 87–96.

☐ Recommended by ACS

Methanol Vapor Retards Aging of PIM-1 Thin Film Composite Membranes in Storage

Ming Yu, Peter M. Budd, et al.

JANUARY 06, 2023

RFAD 🗹

Benzyl-Induced Crosslinking of Polymer Membranes for Highly Selective CO₂/CH₄ Separation with Enhanced Stability

Shouwen Zhu, Jian Jin, et al.

JULY 24, 2022 MACROMOLECULES

READ 🗹

Improving the Blood Compatibility and the Gas Permeability of Polyether Ether Ketone Hollow Fiber Membrane Used for Membrane Oxygenator via Grafting Hydrophilic Compon...

Xiangpu Qin, Pengqing Liu, et al

MAY 29, 2023

ACS APPLIED POLYMER MATERIALS

READ 🗹

Thermal-Oxidative Membranes Based on Block Hydroxyl Polyimide for H, Separation

Yuxuan Feng, Jizhong Ren, et al.

DECEMBER 29, 2021

MACROMOLECULES

READ 🗹

Get More Suggestions >